Two-step breakdown of a local ν=1 quantum Hall state

Masayuki Hashisaka, Koji Muraki, and Toshimasa Fujisawa

Phys. Rev. B **101**, 041303 — Published 22 January 2020

DOI: 10.1103/PhysRevB.101.041303

Two-step breakdown of a local $\nu = 1$ quantum Hall state

Masayuki Hashisaka[1-3,*], Koji Muraki[2], Toshimasa Fujisawa[1]
[1]*Department of Physics, Tokyo Institute of Technology, 2-12-1-H81 Ookayama, Meguro, Tokyo 152-8551, Japan*
[2]*NTT Basic Research Laboratories, NTT Corporation, 3-1 Morinosato-Wakamiya, Atsugi, Kanagawa 243-0198, Japan*
[3]*JST, PRESTO, 4-1-8 Honcho, Kawaguchi, Saitama 332-0012, Japan*

We report quantum Hall effect breakdown of a local filling factor $\nu_{\rm local} = 1$ state formed in a bulk $\nu_{\rm bulk} = 2$ system in an AlGaAs/GaAs heterostructure. When a finite source-drain bias is applied across the local system, the breakdown occurs in two steps. At low bias, quantized conductance through the $\nu_{\rm local} = 1$ system breaks down due to inter-edge electron tunneling. At high bias, the incompressibility of the $\nu_{\rm local} = 1$ system breaks down because the spin gap closes. The two steps are resolved by combining measurements of resistively detected nuclear magnetic resonance and shot noise, which allows one to evaluate electron spin polarization in the local system and spin-dependent charge transport through the system, respectively.

DOI:

In integer quantum Hall (QH) systems, electronic current flows along chiral edge channels[1,2]. When a fine gate is used to form a region with local filling factor $\nu_{\rm local} = 1$ so as to traverse a bulk spin-unpolarized $\nu_{\rm bulk} = 2$ system, only spin-up electrons are transmitted through the local region along the $\nu_{\rm local} = 1$ edge channel. The $\nu_{\rm local} = 1$ system, thus operating as an ideal (spin) filter for edge channels at low bias, has been widely used to study charge and spin dynamics in QH systems, such as spin-charge separation[3], providing insights into edge coherence and energy equilibration. When a high bias voltage is applied, however, inter-edge scattering sets in, which drives the $\nu_{\rm local} = 1$ system out of equilibrium so that it exhibits significant nonlinear behavior that bears a resemblance to the QH effect breakdown in macroscopic samples[4,5]. The occurrence of spin-flip scattering as well as spin-conserved scattering in the QH effect breakdown has been manifested by the dynamic nuclear polarization of the host crystal in both integer and fractional regimes[6-9]. Indeed, resistively detected nuclear magnetic resonance (NMR) has shown that the electron spin polarization decreases under a high bias in both mesoscopic and macroscopic systems[10-13]. On the other hand, inter-edge scattering generates shot noise in mesoscopic systems, from which the spin polarization of the transmitted current can be deduced under the assumption that the scattering event is random partitioning of electrons, i.e., with no correlation[13]. The disagreement between the NMR and shot-noise results found in Ref. 13, in turn, suggests that the charge scattering process generating the shot noise does not directly reflect the electron spin population in the local system.

In this paper, we report a two-step breakdown of a $\nu_{\rm local} = 1$ QH state in a narrow constriction of a $\nu_{\rm bulk} = 2$ system [Fig. 1(a)]. With increasing bias, in the first step, the quantized conductance $G_0 = e^2/h$ (e: elementary charge, h: Plank's constant) of the $\nu_{\rm local} = 1$ system breaks down due to inter-edge electron tunneling. In the second step, the incompressibility of the $\nu_{\rm local} = 1$ system breaks down because the spin gap closes. This is induced by the suppression of the exchange energy at high bias. We show that the deviation between the NMR and shot-noise results reported in the previous paper[13] appears in the second regime. The well-designed combination of the NMR and shot-noise measurements presented in this paper enables us to gain deep insight into the complicated nonlinear response of the $\nu_{\rm local} = 1$ system, thus opening a way to investigate highly nonequilibrium electron dynamics in mesoscopic QH systems.

A schematic of the experiment is shown in Fig. 1(b). The sample was fabricated in a two-dimensional electron system (2DES) in an AlGaAs/GaAs heterostructure (95 nm in depth) with electron density $n_e = 2.5 \times 10^{11}$ cm^{-2} and mobility $\mu = 3.3 \times 10^6$ cm^{2}V^{-1}s^{-1}. Electron temperature T_e of the sample was reduced to 14 mK in a dilution refrigerator (base temperature: 7 mK), and an external magnetic field $B_{\rm ext} = 5.0$ T was applied perpendicular to the 2DES to form the $\nu_{\rm bulk} = 2$ state. The magnetic-field direction was from the back to front of the sample so that the chirality of the edge states was clockwise. A gate voltage $V_{\rm g}$ was applied to the split gate (length: 200 nm, width: 300 nm) to form a narrow constriction (inset), where a $\nu_{\rm local} = 1$ state is formed. We applied a source-drain voltage $V_{\rm in}$ to drive a current $I_{\rm in}$ through the ohmic contact Ω_0. The dc transport characteristics through the constriction were evaluated by measuring backscattered current I_1 through contact Ω_1. In

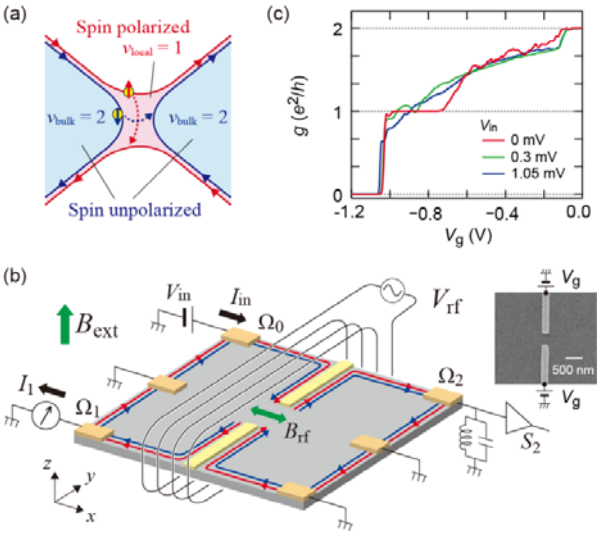

Figure 1. (a) Local $\nu_{\rm local} = 1$ QH system formed in a bulk $\nu_{\rm bulk} = 2$ system. (b) Schematic of experimental setup. (Inset) scanning electron micrograph of the device. (c) Pinch-off traces of the split gate measured at several $V_{\rm in}$ values.

addition to the conductance $G = (I_{in} - I_1)/V_{in} = G_0(T_\uparrow + T_\downarrow)$, we measured the differential conductance $g = dI_{in}/dV_{in} - dI_1/dV_{in}$ using a standard lock-in technique with a small ac modulation of V_{in} (15 μV, 37 Hz). Here, $T_{\uparrow(\downarrow)}$ is the transmission probability for spin-up (-down) electrons. The shot noise was evaluated by measuring current fluctuation $S_2 = \langle(\Delta I_2)^2\rangle$ through contact Ω_2 using an LC circuit and a cryogenic amplifier. The resistively detected NMR of ^{75}As nuclei was measured using a conventional three-step procedure[12-14] by applying a radio-frequency in-plane magnetic field B_{rf} with a four-turn coil. Further details of the measurements are described in **Supplemental material (S.M.)**[15].

The gate voltage V_g dependence of g measured at several V_{in} values is shown in Fig. 1(c). At $V_{in} = 0$ mV, a well-developed $g = e^2/h$ plateau is observed over a wide range of -1.0 V $< V_g < -0.7$ V, indicating spin-resolved transport in the lowest Landau level. The $\nu_{local} = 1$ system is formed in this $g = e^2/h$ plateau region. When V_{in} is increased to 0.3 mV, the $g = e^2/h$ plateau disappears, signaling nonlinear transport through the constriction. When V_{in} is further increased to 1.05 mV, the pinch-off trace changes further to show a monotonic decrease in g with decreasing V_g.

The nonlinear nature of the breakdown becomes more evident by color plotting g in the V_{in}-V_g plane [Fig. 2(a)]. The $g = e^2/h$ plateau, which appears as a white area around $V_{in} = 0$ mV extending over -1.0 V $< V_g < -0.7$ V, is suddenly terminated at $|V_{in}| = 0.25$ mV. To provide more details, in Fig. 2(b) we plot g traces at several fixed V_g values. The $g = e^2/h$ plateau appears as accumulated traces around $|V_{in}| = 0$ mV. Complex nonlinear behavior is seen at $|V_{in}| > 0.25$ mV. For example, at $V_g = -0.96$ V (red solid curve), g first starts to increase from e^2/h at $|V_{in}| \cong 0.25$ mV and then begins to decrease before it saturates at $g \cong 0.85e^2/h$ for $|V_{in}| > 0.7$ mV. It should be noted that the nonlinear behavior is seen in the regime where the bias energy $|eV_{in}|$ is considerably larger than the Zeeman energy $E_Z = |g^*\mu_B B|$ ($\cong 0.12$ meV) and much smaller than the exchange-enhanced spin gap $E_Z + E_{ex}$ ($\cong 2$ meV) in bulk 2DES samples[16-18].

The nonlinear behavior in the low-bias regime ($|V_{in}| <$ 0.45 mV) can be understood by considering the inter-edge electron tunneling illustrated in Figs. 2(c) and 2(d). The tunneling is manifested in the V_g dependence of g. For example, when V_g is slightly increased from –0.96 to –0.90 V [blue solid line in Fig. 2(b)], g starts to increase from e^2/h at a lower $|V_{in}|$. This indicates the enhanced forward scattering of spin-down electrons, which can be explained by the shorter distance between the $\nu_{bulk} = 2$ edges at a higher V_g [Fig. 2(c)]. When V_g is slightly lowered to –0.98 V instead (green solid line), g turns to decrease from e^2/h, reflecting the reduced distance between the $\nu_{local} = 1$ edges and the resultant enhanced backscattering of spin-up electrons [Fig. 2(d)].

To unravel the complex behavior at high bias ($|V_{in}| >$ 0.45 mV), we analyze the shot noise and NMR results measured over the entire $|V_{in}|$ range. Figures 3(a), (b), and (c) plot, as a function of V_{in}, the results of three different

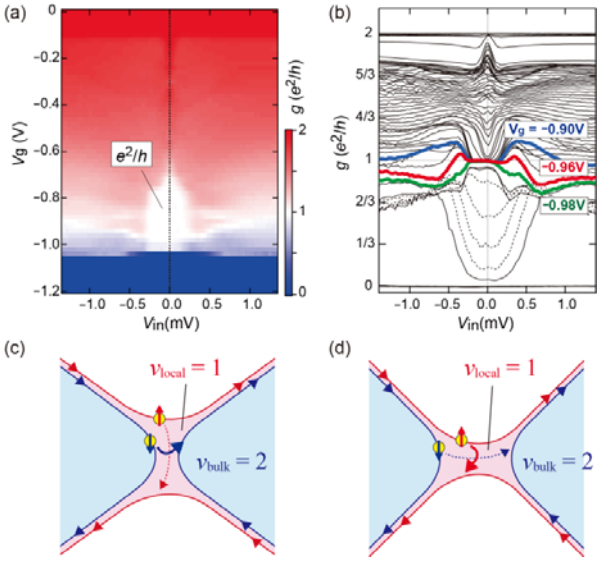

Figure 2. (a) Color plot of g as a function of V_g and V_{in}. (b) V_{in} dependence of g measured in 20-mV (solid lines: 0 V $\le V_g \le -1.1$ V) and 4-mV (dashed lines: -1.024 V $\le V_g \le -1.036$ V) steps of V_g. Each trace was measured by sweeping V_{in} with a slow speed of 0.067 mV/min. (c)(d) Schematics of the inter-edge tunneling at (c) high and (d) low V_g.

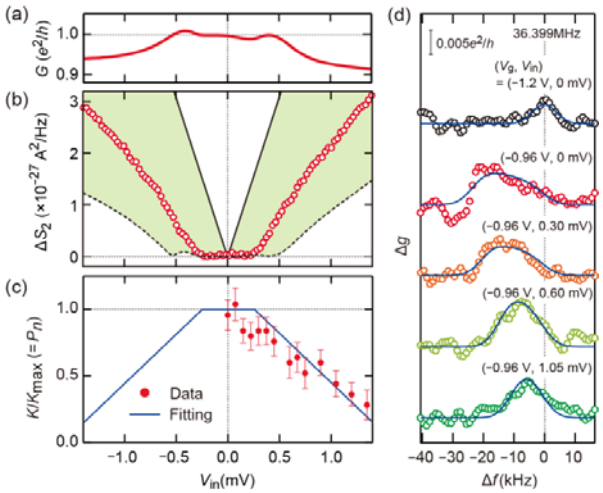

Figure 3. (a) V_{in} dependence of G at $V_g = -0.96$ V. (b) V_{in} dependence of ΔS_2. Solid and dashed curves are S_{shot} calculated assuming $F_c = 1$ for fully spin-degenerate and spin-resolved transport, respectively. In general cases, S_{shot} appears in the green area. (c) V_{in} dependence of $P_n = K/K_{max}$. Error bars indicate fitting errors for the NMR spectra in Fig. 3(d). (d) Representative NMR spectra. Blue lines are fitted curves.

measurements, (a) conductance G, (b) excess current noise $\Delta S_2 = S_2(V_{in}) - S_2(0)$, and (c) NMR Knight shift K, which were obtained at the same V_g of –0.96 V. The nonlinear behavior of G, similar to that of g, is evident in Fig. 3(a), where G first increases at $|V_{in}| \cong 0.25$ mV and then begins

to decrease above $|V_{in}| \cong 0.45$ mV. ΔS_2, which vanishes at low $|V_{in}|$, starts to increase above $|V_{in}| \cong 0.25$ mV [Fig. 3(b)]. K monotonically decreases with increasing $|V_{in}|$ [Fig. 3(c)].

We first compare the observed V_{in} dependence of ΔS_2 with the theoretical shot noise expected for the two limiting cases—spin-degenerate and fully spin-resolved transport—shown as the solid and dashed curves in Fig. 3(b), respectively. Shot-noise power can be expressed as[19]

$$S_{shot} = FS_0 = F \times 2eG_0V_{in}\left[\coth\left(\frac{eV_{in}}{2k_BT_e}\right) - \frac{2k_BT_e}{eV_{in}}\right], \quad (1)$$

where k_B is the Boltzmann constant and the factor F represents the shot-noise reduction due to various mechanisms. To disentangle spin-dependent mechanisms from other ones, here we express F as $F = F_sF_c$, with $F_s = \Sigma_\sigma T_\sigma(1 - T_\sigma)$ representing spin-dependent mechanism ($\sigma = \uparrow$or $\downarrow$). The factor F_c accounts for other mechanisms, such as the anti-bunching of tunneling electrons. For the moment, we set $F_c = 1$, assuming the electron scattering at the constriction to be random partitioning. The S_{shot} vs V_{in} curves for (i) spin-degenerate and (ii) fully spin-resolved transport, shown in Fig. 3(b), were obtained by setting (i) $T_\uparrow = T_\downarrow = G/2G_0$ so that $F_s = 2(G/2G_0)[1 - (G/2G_0)]$ and (ii) $F_s = [G/G_0 - \text{floor}(G/G_0)]\{1 - [G/G_0 - \text{floor}(G/G_0)]\}$, respectively. In general cases, S_{shot} takes intermediate values between the two curves (green area). Indeed, the measured ΔS_2 values fall inside this area.

In the linear-response regime ($|V_{in}| < 0.25$ mV), we observe $\Delta S_2 \cong 0$, in line with spin-resolved transport ($F_s \cong 0$, dashed curve). This unambiguously shows that the transport through the $\nu_{local} = 1$ region is fully spin resolved. As $|V_{in}|$ is increased, ΔS_2 starts to increase at $|V_{in}| = 0.25$ mV. Note that this threshold for finite shot noise is considerably lower than that expected for the spin-resolved transport (0.5 mV, dashed curve). This indicates that the system has entered a different regime where both spin-up and spin-down electrons are involved in the inter-edge scattering. We evaluate the spin polarization $P_T \equiv (T_\uparrow - T_\downarrow)/(T_\uparrow + T_\downarrow)$ of the transmitted current from the shot-noise result. This is possible when the scattering event is random partitioning, i.e. $F_c = 1$. We calculate the quantity $\alpha_{shot} = (T_\uparrow' - T_\downarrow')/(T_\uparrow' + T_\downarrow')$, where $T_\uparrow'$ and $T_\downarrow'$ are the quantities obtained by solving the coupled equations $T_\uparrow' + T_\downarrow' = G/G_0$ and $\Sigma_\sigma T_\sigma'(1 - T_\sigma') = \Delta S_2/S_0$. Note that when $F_c = 1$, $T_{\uparrow(\downarrow)}' = T_{\uparrow(\downarrow)}$ so that $\alpha_{shot} = P_T$. In Fig. 4(a), the obtained α_{shot} is plotted as a function of V_{in}. The plot reveals the existence of thresholds at $V_{in} \cong 0.25$ mV ($\equiv V_{th1}$) and 0.45 mV ($\equiv V_{th2}$). At $V_{in} = V_{th1}$, α_{shot} starts to decrease from 1 and then, at $V_{in} = V_{th2}$, it stops decreasing linearly and starts saturating toward $\alpha_{shot} \cong 0.9$. We note that V_{th1} and V_{th2} are close to the V_{in} values at which G starts to increase and decrease, respectively [Fig. 3(a)]. Below, we compare α_{shot} with the spin polarization evaluated from NMR measurements.

The Knight shift K of the NMR is proportional to the electron-spin imbalance $\Delta n = n_\uparrow - n_\downarrow$ in the constriction, where $n_\uparrow$ and $n_\downarrow$ are spin-up and spin-down electron densities, respectively[12-14]. Here, we assume $n_\uparrow + n_\downarrow$ to be constant at a given V_g and evaluate the spin polarization $P_n \equiv (n_\uparrow - n_\downarrow)/(n_\uparrow + n_\downarrow)$ at $V_g = -0.96$ V as $P_n = K/K_{max}$, where K_{max} is the Knight shift for the fully spin-polarized case. Figure 3(d) shows representative NMR spectra and fitted curves [for the fitting function, see eq. (S1) in **S.M.**[15]]. When the 2DES in the local region is completely depleted at $V_g = -1.2$ V, a peak is observed at 36.399 MHz, which we use as the reference resonance frequency f_{ref} of ^{75}As nuclei at $B_{ext} = 5.0$ T. The spectra obtained at $V_g = -0.96$ V show finite shifts to lower frequencies. From the fitting at $V_{in} \cong 0$ mV, where the 2DES in the constriction is fully spin polarized, $K_{max} \cong 25$ kHz is obtained. When V_{in} is increased, the NMR spectra shift to a higher frequency toward f_{ref}, indicating a decrease in K ($\propto P_n$) due to the tunneling of spin-down electrons across the constriction. Figure 3(c) summarizes the V_{in} dependence of K/K_{max} ($= P_n$). We fit the data at $V_{in} > 0.25$ mV by a linear function ($P_n = -772\,|V_{in}| + 1.17$) with the constraint that $P_n = 1$ in the linear-response regime ($|V_{in}| < 0.25$ mV)[20]. Thus, we obtain P_n over the entire V_{in} range, as shown by the blue curve.

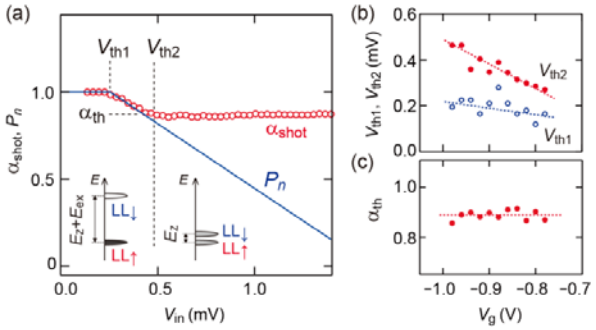

Figure 4. (a) V_{in} dependence of α_{shot} and P_n. (Inset) schematics of the lowest Landau levels in the constriction at low- (left) and high-bias (right) regimes. (b) V_g dependence of V_{th1} and V_{th2}. (c) V_g dependence of α_{th}.

We compare the V_{in} dependence of α_{shot} and P_n in Fig. 4(a). At $V_{in} < V_{th2}$, α_{shot} agrees well with P_n, suggesting $\alpha_{shot} = P_T \cong P_n$ in this regime. In contrast, α_{shot} tends to saturate at $\alpha_{shot} \cong 0.9$ for $V_{in} > V_{th2}$, while P_n monotonically decreases with increasing V_{in}. The deviation between α_{shot} and P_n at high bias clearly shows that the electron dynamics at low and high bias are distinct from each other.

Figures 4(b) and 4(c) present the V_g dependence of V_{th1}, V_{th2}, and α_{th} (α_{shot} value at $V_{in} = V_{th2}$) extracted from the shot-noise results (see **S.M.** for details of the analysis[15]). While V_{th1} and V_{th2} vary depending on V_g, α_{th} remains almost constant at $\alpha_{th} \cong 0.9$ independent of V_g. This implies that the second step of the breakdown is triggered when the spin polarization drops to $P_n \cong 0.9$ due to spin-down electron tunneling. The decrease in P_n leads to the suppression of the exchange-enhanced spin gap [inset in Fig. 4(a)]. As a result, the incompressible $\nu_{local} = 1$ state breaks down at $|V_{in}| > V_{th2}$, leading to highly

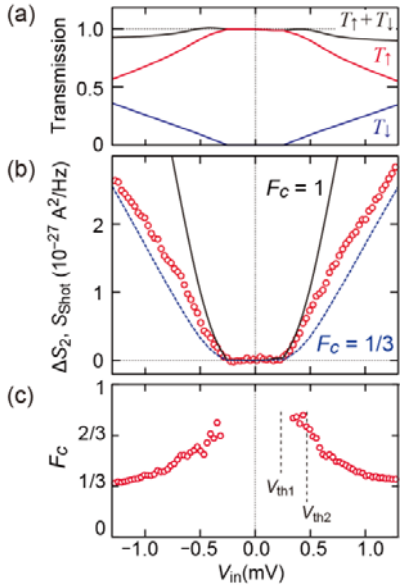

Figure 5. (a) V_{in} dependence of $T_\uparrow$, $T_\downarrow$, and $T_\uparrow + T_\downarrow$ estimated assuming $P_n = P_T$. (b) ΔS_2 [same data as in Fig. 3(b)] and S_{shot} curves for $F_c = 1$ and $F_c = 1/3$ calculated using $T_\uparrow$ and $T_\downarrow$ in Fig. 5(a). (c) V_{in} dependence of F_c.

nonequilibrium electron dynamics that is distinct from the inter-edge electron tunneling. The complete disappearance of the $g = e^2/h$ plateau at $V_{in} = 1.05$ mV supports the breakdown picture [Fig. 1(c)]. In addition, the bias-induced exchange-energy suppression can explain why eV_{th1} and eV_{th2} are larger than the Zeeman energy and smaller than the exchange-enhanced spin-gap energy.

We observe that V_{th2} is significantly enhanced with decreasing V_g, whereas V_{th1} increases only slightly. The strong V_g dependence of V_{th2} is linked to the V_g dependence of P_n. That is, at lower V_g, higher $|V_{in}|$ is required to attain a sufficient spin-down tunneling rate [Fig. 3(d)]. This is consistent with the observation that under a finite bias K increases with decreasing V_g (see Fig. S5 in **S.M.**[15]). In contrast, V_{th1} depends on V_g only weakly because it indicates the onset of inter-edge tunneling for either spin-up or spin-down electrons.

In the second breakdown regime, the deviation between P_n and α_{shot} suggests $F_c < 1$ at $V_{in} > V_{th2}$. In the following, we analyze the shot-noise data at $V_g = -0.96$ V, with the $F_c = 1$ constraint removed and, instead, with the assumption $P_n = P_T$ introduced. With this assumption, $T_\uparrow$ and $T_\downarrow$ can be calculated from the measured P_n and G. The $T_\uparrow$ and $T_\downarrow$ values obtained in this way are plotted in Fig. 5(a) as a function of V_{in}, along with $T_\uparrow + T_\downarrow$. We use these $T_\uparrow$ and $T_\downarrow$ traces to calculate F_s as a function of V_{in}, which in turn allows one to simulate S_{shot} for arbitrary F_c. In Fig. 5(b), we compare the S_{shot} curves simulated for $F_c = 1$ and $F_c = 1/3$ with the experimental ΔS_2 data shown in Fig. 3(b). In this plot, we again observe the two-step behavior of the breakdown: in the low-bias regime ($V_{th1} < |V_{in}| < V_{th2}$), ΔS_2 follows the $F_c = 1$ shot-noise curve; and at higher bias ($V_{th2} < |V_{in}|$), it deviates from the $F_c = 1$ curve and approaches the $F_c = 1/3$ curve. Figure 5(c) summarizes the V_{in} dependence of F_c obtained from the relation $F_c = \Delta S_2/F_s S_0$. Above $|V_{in}| = V_{th2}$, we find a significant decrease in F_c from $F_c \cong 1$ to 1/3. Thus, the nonequilibrium transport in the second breakdown regime can be evaluated as a change in F_c.

Although electron dynamics in the second nonequilibrium regime is unclear, the shot-noise results provide important insights into the second breakdown process. One possible scenario inferred from the experimental data is the formation of compressible electron liquid. Transport through the compressible liquids of nearly half-filled spin-up and spin-down Landau levels may cause the $F_c \cong 1/3$ shot noise[21-25]. Another possible scenario is the fractional charge tunneling through the local fractional QH system[26-29]. For both scenarios, the incompressibility of the $\nu_{local} = 1$ state needs to break down. Further experimental and theoretical studies will clarify the electron dynamics in the highly nonequilibrium regime.

In summary, we have investigated the nonlinear behavior of the $\nu_{local} = 1$ state formed in the $\nu_{bulk} = 2$ system. A two-step breakdown process was successfully identified through NMR and shot-noise measurements. In the first step, inter-edge electron tunneling breaks down the $\nu_{local} = 1$ conductance plateau. The second step is caused by the closing of the spin gap due to the suppression of the exchange energy. Shot-noise reduction toward $F_c \cong 1/3$ is observed in the second regime, indicating the breakdown of the incompressible $\nu_{local} = 1$ state.

We appreciate technical support from T. Endo and fruitful discussions with K. Chida, K. Kobayashi, N. Kumada, and Y. Tokura. This study was supported by Grants-in-Aid for Scientific Research (JP16H06009, JP15H05854, JP26247051), JST PRESTO Grant Number JP17940407, and the Nanotechnology Platform Program (Tokyo Institute of Technology).

* masayuki.hashisaka.wf@hco.ntt.co.jp

[1] K. von Klitzing, G. Dorda, and M. Pepper, New method for high-accuracy determination of the fine-structure constant based on quantized Hall resistance. *Phys. Rev. Lett.* **45**, 494-497 (1980).
[2] Z. F. Ezawa, Quantum Hall Effects: Field Theoretical Approach and Related Topics, World Scientific, Singapore, 2008 and references therein.
[3] M. Hashisaka, N. Hiyama, T. Akiho, K. Muraki and T. Fujisawa, Waveform measurement of charge- and spin-density wavepackets in a chiral Tomonaga–Luttinger liquid. *Nat. Phys.* **13**, 559-562 (2017).
[4] G. Nachtwei, Breakdown of the quantum Hall effect. *Physica. E* **4**, 79-101 (1999).
[5] C. Dillard, X. Lin, M. A. Kastner, L. N. Pfeiffer, and K. W. West, Breakdown of the integer and fractional quantum

Hall states in a quantum point contact. *Physica E* **47**, 290-296 (2013).
[6] K. R. Wald, L. P. Kouwenhoven, P. L. McEuen, N. C. van der Vaart, and C. T. Foxon, Local Dynamic Nuclear Polarization Using Quantum Point Contacts. *Phys. Rev. Lett.* **73**, 1011-1014 (1994).
[7] D. C. Dixon, K. R. Wald, P. L. McEuen, and M. R. Melloch, Dynamic nuclear polarization at the edge of a two-dimensional electron gas. *Phys. Rev. B* **56**, 4743-4750 (1997).
[8] G. Yusa, K. Muraki, K. Takashina, K. Hashimoto, and Y. Hirayama, Controlled multiple quantum coherences of nuclear spins in a nanometre-scale device, *Nature* **434**, 1001-1005 (2005).
[9] S. Hennel, B. A. Braem, S. Baer, L. Tiemann, P. Sohi, D. Wehrli, A. Hofmann, C. Reichl, W. Wegscheider, C. Rössler, T. Ihn, K. Ensslin, M. S. Rudner, and B. Rosenow, Nonlocal Polarization Feedback in a Fractional Quantum Hall Ferromagnet. *Phys. Rev. Lett.* **116**, 136804-1-5 (2016).
[10] A. Córcoles, C. J. B. Ford, M. Pepper, G. A. C. Jones, H. E. Beere, and D. A. Ritchie, Nuclear spin coherence in a quantum wire. *Phys. Rev. B* **80**, 115326 (2009).
[11] M. H. Fauzi, A. Singha, M. F. Sahdan, M. Takahashi, K. Sato, K. Nagase, B. Muralidharan, and Y. Hirayama, Resistively detected NMR line shapes in a quasi-one-dimensional electron system. *Phys. Rev. B* **95**, 241404(R)-1-5 (2017).
[12] S. Masubuchi, K. Hamaya, and T. Machida, Knight shift detection using gate-induced decoupling of the hyperfine interaction in quantum Hall edge channels, *Appl. Phys. Lett.* **89**, 062108-1-3 (2006).
[13] K. Chida, M. Hashisaka, Y. Yamauchi, S. Nakamura, T. Arakawa, T. Machida, K. Kobayashi, and T. Ono, Shot noise induced by electron-nuclear spin-flip scattering in a nonequilibrium quantum wire. *Phys. Rev. B* **85**, 041309(R)-1-4 (2012).
[14] M. Kawamura, K. Ono, P. Stano, K. Kono, and T. Aono, Electronic Magnetization of a Quantum Point Contact Measured by Nuclear Magnetic Resonance. *Phys. Rev. Lett.* **115**, 036601-1-5 (2015).
[15] See Supplemental Material at *** for more information on the two-terminal resistance of the 2DES, dc transport characteristics through the split gate, details of the experimental techniques, and V_g dependence of the Knight shift and shot noise.
[16] R. J. Nicholas, R. J. Haug, K. v. Klitzing, and G. Weimann, Exchange enhancement of the spin splitting in a GaAs-$Ga_xAl_{1-x}As$ heterojnnction. *Phys. Rev. B* **37**, 1294-1302 (1988).
[17] A. Usher, R. J. Nicholas, J. J. Harris, and C. T. Foxon, Observation of magnetic excitons and spin waves in activation studies of a two-dimensional electron gas. *Phys. Rev. B* **41**, 1129-1134 (1990).
[18] V. T. Dolgopolov, A. A. Shashkin, A. V. Aristov, D. Schmerek, W. Hansen, J. P. Kotthaus, and M. Holland, Direct Measurements of the Spin Gap in the Two-Dimensional Electron Gas of AlGaAs-GaAs Heterojunctions. *Phys. Rev. Lett.* **79**, 729-732 (1997).
[19] Y. M. Blanter and M. Büttiker, Shot noise in mesoscopic conductors, *Phys. Rep.* **336**, 1 (2000).
[20] The Knight shift starts to decrease at $|V_{in}| \cong 0.1$ mV somewhat smaller than V_{th1} (= 0.25 mV) [Fig. 3(c)]. This is possibly because the experimental environment in the NMR measurement is slightly different from that in the shot-noise measurement. That is, in the NMR measurement, nuclear spins are polarized and the rf magnetic field is irradiated. Although the rf irradiation increases T_e during the NMR experiment, the increase is small enough to keep the main features of the pinch-off characteristics of the split gate unchanged (see Fig. S5 in S.M.[15]). If the measurement was performed in the same environment as in the shot-noise measurement, we expect that P_n would remain constant below V_{th1}, as shown by the blue line.
[21] C. W. J. Beenakker and M. Büttiker, Suppression of shot noise in metallic diffusive conductors. *Phys. Rev. B* **46**, 1889-1892R (1992).
[22] K. E. Nagaev, Influence of electron-electron scattering on shot noise in diffusive contact. *Phys. Rev. B* **52**, 4740-4743 (1995).
[23] V. I. Kozub and A. M. Rudin, Shot noise in mesoscopic diffusive conductors in the limit of strong electron-electron scattering. *Phys. Rev. B* **52**, 7853-7856 (1995).
[24] F. von Oppen, Shot noise in the half-filled Landau level. *Phys. Rev. B* **56**, 9674-9683 (1997).
[25] A. H. Steinbach, J. M. Martinis, and M. H. Devoret, Observation of Hot-Electron Shot Noise in a Metallic Resistor, *Phys. Rev. Lett.* **76**, 3806-1-4 (1996).
[26] S. Roddaro, V. Pellegrini, F. Beltram, G. Biasiol, L. Sorba, R. Raimondi, and G. Vignale, Nonlinear Quasiparticle Tunneling between Fractional Quantum Hall Edges, *Phys. Rev. Lett.* **90**, 046805-1-4 (2003).
[27] S. Roddaro, V. Pellegrini, F. Beltram, G. Biasiol, and L. Sorba, Interedge Strong-to-Weak Scattering Evolution at a Constriction in the Fractional Quantum Hall Regime, *Phys. Rev. Lett.* **93**, 046801-1-4 (2004).
[28] S. Roddaro, N. Paradiso, V. Pellegrini, G. Biasiol, L. Sorba, and F. Beltram, Tuning Nonlinear Charge Transport between Integer and Fractional Quantum Hall States, *Phys. Rev. Lett.* **103**, 016802 (2009).
[29] M. Hashisaka, T. Ota, K. Muraki, and T. Fujisawa, Shot-noise evidence of fractional quasiparticle creation in a local fractional quantum Hall state, *Phys. Rev. Lett.* **114**, 056802-1-5 (2015).